Fluidmechanical Damping Analysis of Resonant Micromirrors with Out-of-plane Comb Drive

Thomas Klose[1], Holger Conrad[2], Thilo Sandner*,[1], and Harald Schenk[1]
[1]Fraunhofer Institute Photonic Microsystems (FhG-IPMS),
[2]TU Dresden, Semiconductor and Microsystems Technology Laboratory
*Corresponding author: Maria-Reiche-Str. 2, 01109 Dresden, Germany, thilo.sandner@ipms.fraunhofer.de

Abstract: Damping is the limiting factor for the reachable maximum deflection. Thus, it is a very important issue for resonant microsystems. In this paper, we present a damping model for out-of-plane comb driven resonant micromirrors. The basic concept of this model is to attribute viscous damping in the comb gaps as the dominant contributor of damping moments. The model is extended by findings from a fluidmechanical FEM model of an electrode finger and the moving mirror plate with a cavity underneath. It also considers effects from pressure and temperature changes. The results are verified and discussed in the context of experimental data. The primary goal of damping analysis and optimization is to minimize power consumption and to reduce driving voltage. The presented methods and models create the prerequisites for this task.

Keywords: MEMS, Micromirror, comb drive, Damping, Navier-Stokes, FEM.

1 Introduction

The resonant micromirrors developed at Fraunhofer IPMS in Dresden are electrostatically driven MEMS devices. The driving moment is supplied by an out-of-plane comb drive which is realized by structuring the mirror plate along its edge (Fig. 1). The micromirrors can be actuated using a pulse-shaped voltage with a pulse frequency approximately twice the resonance frequency of the mechanical system. The achievable maximum deflection angle for a certain device is determined only by the ratio of the energy feed-in and the energy feed-out. The energy feed-in is determined by the driving voltage, the driving scheme (e.g. frequency, duty-cycle), and the change of the capacitance of the comb drive during the oscillation. The energy feed-out is determined by the damping of the system. Since the devices are processed in monocrystalline silicon and are operated in ambient pressure, fluidmechanical damping is considered to be the only relevant.

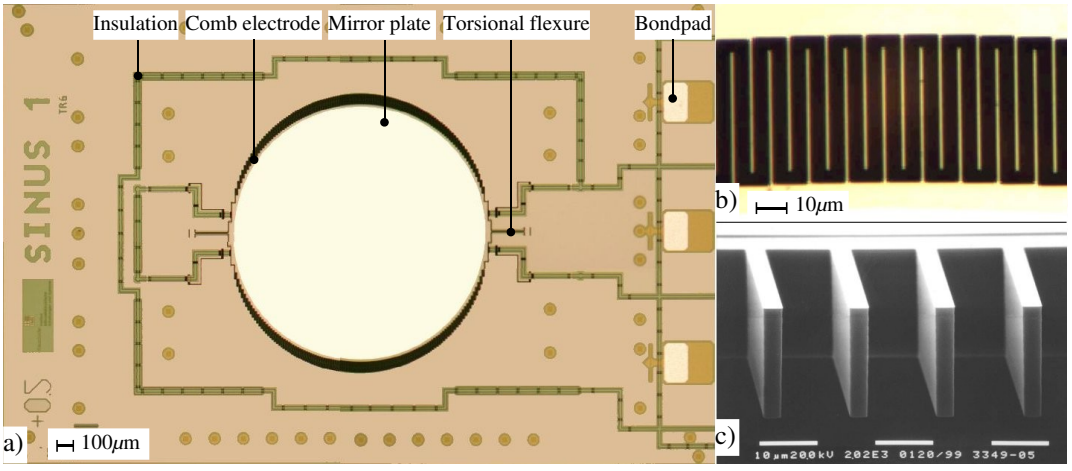

Figure 1: Micromachined scanning micromirror with out-of-plane comb drive actuation. a) Microscopic photograph of a die, b) Detail view of the comb drive, c) REM image of the finger electrodes.

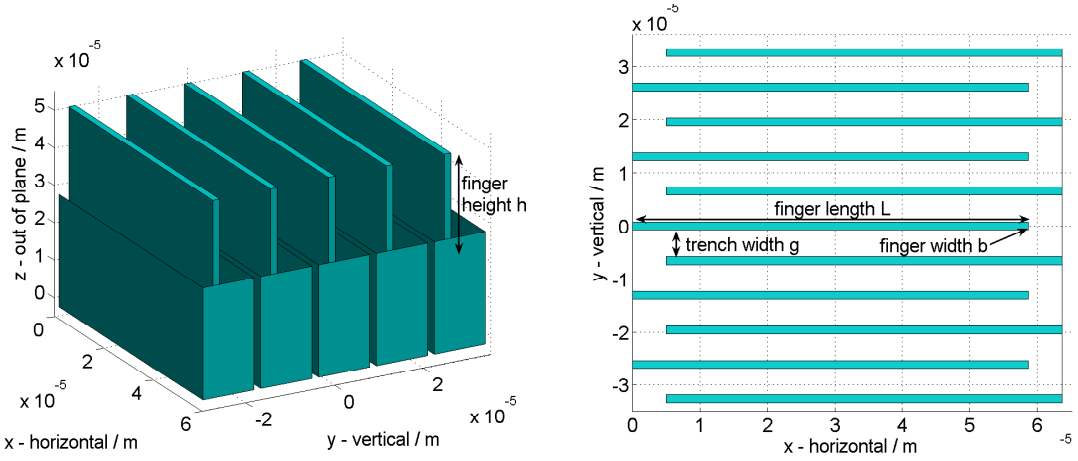

Figure 2: Schematic configuration of the out-of-plane comb drive and its orientation in the model's coordinate system

For description of the oscillation properties damping effects have to be thoroughly understood. In this paper we present a damping analysis of out-of-plane comb driven resonant micromirrors. It is based on parameterized fluidmechanical 3D FEM models which are realized in *COMSOL Multiphysics*^{TM} utilizing the application mode *Incompressible Navier-Stokes*.

The analysis includes slide-film damping effects within the electrostatic comb drive as well as squeeze and drag damping affecting the mirror plate. Within the validity range of theories of continuous flow, pressure and temperature effects are considered by introducing an effective dynamic viscosity.

A dedicated damping structure is available for the verification of simulation results and the extraction of empiric data. It is an one-dimensional micromirror with a circular mirror plate, with a diameter of 1.5 mm, and an oscillation frequency of 1 kHz (Fig. 1). To compare the properties and efficiencies of different comb geometries, six different comb designs, varying the dimensions of the electrode fingers and the widths of the trenches between the electrodes were realized [4]. The reference damping structure shown in Fig. 1 has a finger length of $L = 58.5\,\mu$m, a finger width of $b = 1.5\,\mu$m and a trench width of $g = 5\,\mu$m. The height of the mirror plate and the comb structure is $h = 30\,\mu$m. Figure 2 shows the schematic configuration of the out-of-plane comb drive. Furthermore it implies the description of dimensions used in this paper.

The transient behavior of resonant micromirrors can be described by an equilibrium of torques which results in a second order ordinary differential equation:

$$J\,\ddot{\theta} + M_{\mathrm{d}}(\dot{\theta},\theta) + k\,\theta = M_{\mathrm{el}}(\theta,U) \qquad (1)$$

with J as moment of inertia of the oscillating structure, $\theta = f(t)$ as deflection angle, $M_{\mathrm{d}}(\dot{\theta},\theta)$ as damping torque, k as torsional spring constant, and $M_{\mathrm{el}}(\theta,U)$ as electrostatic torque which is generated by the out-of-plane comb drive. This driving torque depends on the deflection angle and the driving voltage U. Since the terms $M_{\mathrm{d}}(\dot{\theta},\theta)$ and $M_{\mathrm{el}}(\theta,U)$ are strongly nonlinear, the exact solution for θ can only be computed with numerical methods. For oscillation amplitudes which are in the range of several degrees applies

$$\left|J\,\ddot{\theta}\right| + \left|k\,\theta\right| \gg \left|M_{\mathrm{d}}(\dot{\theta},\theta)\right| + \left|M_{\mathrm{el}}(\theta,U)\right|$$

Thus, the equilibrium solution of θ can be assumed to be sinusoidal:

$$\theta \approx \hat{\theta}\,\sin(2\pi f\,t + \varphi) \qquad (2)$$

with f as oscillation frequency, φ as phase shift and $\hat{\theta}$ as oscillation amplitude, which still depends on $M_{\mathrm{d}}(\dot{\theta},\theta)$ and $M_{\mathrm{el}}(\theta,U)$. Afterwards the phase shift φ is assumed to be zero.

To prove the damping model and its range of validity it is necessary to compare simulation results with experimental data. Since the transient characteristics of the damping moment can not be measured

directly, a mean damping coefficient is introduced:

$$D = \frac{1}{T} \int_0^T \frac{M_\mathrm{d}(\dot{\theta}, \theta)}{\dot{\theta}} \, \mathrm{d}t \, , \qquad T = \frac{1}{f} \quad (3)$$

This mean damping coefficient can be measured[4]. Thus, it is possible to verify simulation results with experimental data.

2 Governing equations

2.1 Flow properties

For determination of valid approaches and models which can be applied to a given fluidmechanical problem there are several physical measures available.

The Knudsen-number measures the ratio between mean free path length within the fluid and a characteristic geometrical length of the structure. It is used to determine whether the continuum mechanics formulation of fluid dynamics can be used. It is defined to

$$\mathrm{Kn} \; = \; \frac{\mathcal{L}}{d} \quad (4)$$

with $\mathcal{L}$ as mean free path length and d as characteristic structure length.

The continuum condition of Navier-Stokes equations is considered to be fulfilled if $\mathrm{Kn} < 0.1$. With the definition of mean free path length [1] the following condition for temperature and pressure of the fluid can be deduced:

$$\frac{p}{T} \; > \; \left. \frac{k}{\sqrt{2}\,\pi\,\mathrm{Kn}\,d\,\sigma^2} \right|_{\mathrm{Kn}<0.1} \quad (5)$$

With T as absolute temperature, p as ambient pressure, k as Boltzmann constant, and σ as molecule diameter of the fluid.

Assuming a characteristic length of $d = g = 5\,\mu\mathrm{m}$, a maximum absolute temperature of 333 K ($\approx 60\,^\circ\mathrm{C}$), and a molecule diameter of 0.35 nm (nitrogen), the continuum condition is fulfilled for ambient pressures with $p > 1.7 \cdot 10^4\,\mathrm{Pa}$.

Navier-Stokes equations with *no-slip* boundary conditions are only valid if the additional condition $\mathrm{Kn} < 10^{-3}$ is fulfilled. For larger Knudsen numbers a slip occurs at the interface between structure and fluid which has to be considered by the model. This can be done by introducing a modified (effective) dynamic viscosity [6]:

$$\eta_\mathrm{eff} \; := \; \frac{\eta}{1 + f(\mathrm{Kn})} \quad (6)$$

It should be noted that differently from the dynamic viscosity η the effective dynamic viscosity depends on the temperature as well as the pressure of the fluid. Since the Knudsen number depends on the local geometrical properties of the structure (characteristic length) the effective dynamic viscosity is also a function of location.

It was shown in earlier publications [4, 2] that for micromechanical devices the empirical approximation of Knudsen is a good choice for the function $f(\mathrm{Kn})$:

$$f(\mathrm{Kn}) := \frac{Z\,\mathrm{Kn}}{0.1474} \, , \quad Z = \frac{\mathrm{Kn} + 2.507}{\mathrm{Kn} + 3.095} \quad (7)$$

The Reynolds number of a flow is used to determine whether it is laminar or turbulent. It is defined to

$$\mathrm{Re} \; = \; \frac{\rho_\mathrm{m}}{\eta}\, u\, d \quad (8)$$

With ρ_m as density and u as characteristic velocity of the fluid [1]. The maximum Reynolds number is determining the properties of the flow. Is a critical value $\mathrm{Re}_\mathrm{cr} \approx 2000$ exceeded, turbulences appear. Otherwise the flow is laminar.

Considering the geometrical properties it can be shown that the maximum Reynolds number of a micromirror with out-of-plane comb drive can be denoted as [2]:

$$\max \mathrm{Re} \; = \; \frac{\pi\,\rho_m}{\eta}\, \theta\, f\, D\, d \quad (9)$$

With D as diameter of the mirror plate. Even in worst case scenarios (large, fast oscillating mirror) the Reynolds number does not exceed a value of 100. Thus, theories of laminar flow can be applied without limitations.

The Mach number indicates the ratio of inertia forces and compression forces. This corresponds to the quotient of flow velocity and the speed of sound c within the medium:

$$\mathrm{Ma} \; = \; \frac{u}{c} \quad (10)$$

Is the condition $\mathrm{Ma} < 0.3$ fulfilled, compression effects can be neglected. Since the maximum Mach number which occurs within

a flow at typical micromirrors with out-of-plane comb drive is in the range of < 0.1 [2] the fluidmechanical problem can be solved using simplified (incompressible) NAVIER-STOKES equations.

2.2 General flow model

According to the findings in the prior section the fluidmechanical damping of a micromirror with out-of-plane comb drive can be described by incompressible NAVIER-STOKES equations with *slip correction*:

$$\begin{aligned} \rho_m \left(\frac{\partial \vec{u}}{\partial t} + (\vec{u} \cdot \nabla)\vec{u} \right) &= -\nabla p + \eta_{\text{eff}} \, \Delta \vec{u} \\ \nabla \cdot \vec{u} &= 0 \\ \vec{u}_{\text{bc}} &= \vec{v}_{\text{bc}} \end{aligned} \tag{11}$$

Thereby $p = f(x, y, z)$ is the pressure and $\vec{u} = \vec{f}(x, y, z)$ is the velocity of the fluid; $\vec{u}_{\text{bc}}$ and $\vec{v}_{\text{bc}}$ are the flow velocity at the interface between fluid and structure and the velocity of the structure itself.

The obstruction of a moving structure in a fluid can be determined from the results of Eq. (11). The effective damping force results from integration of pressure p over the interfaces (normal component) and the velocity gradient in direction of the interface's normal $\frac{\partial \vec{u}}{\partial \vec{n}_0}$ (tangential component):

$$\vec{F}_{\text{d}} = \iint\limits_{(A)} p \, \vec{n}_0 \, dA + \iint\limits_{(A)} \eta_{\text{eff}} \, \frac{\partial \vec{u}}{\partial \vec{n}_0} \, dA \tag{12}$$

Now the damping torque, effecting a tilting mirror plate can be expressed by:

$$\vec{M}_{\text{d}} = \iint\limits_{(A)} \vec{r} \times d\vec{F}_{\text{d}} \tag{13}$$

With $\vec{r}$ as position vector which is always orthogonal to the rotation axis of the tilting mirror.

3 Theory

3.1 Damping of comb drive

It has been shown that damping of micromirrors with out-of-plane comb drive is dominated by fluidmechanical interaction within the comb structure [4]. To describe these damping mechanisms it is useful to distinguish three different states of the electrodes [2]:

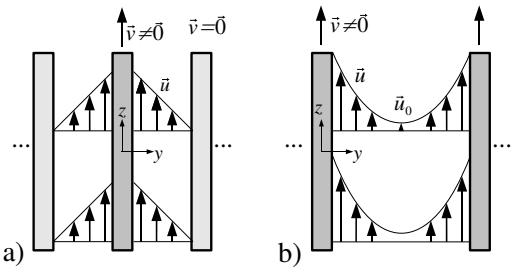

Figure 3: Flow profiles between driving electrodes. a) engaged, b) disengaged state

$\theta \approx 0$ The comb structure is fully engaged. Since the distance of the electrodes is small in comparison to the length and height, the flow between them can be considered as COUETTE flow, indicated by a linear velocity profile (Fig. 3a, [3, 1]). According to Eq. (12), the damping force can be expressed by:

$$\vec{F}_{\text{d}} \approx \vec{F}_{\text{Couette}} = -\eta_{\text{eff}} \, \frac{A_{\text{s}}}{g} \, \vec{v} \tag{14}$$

With $A_{\text{s}} \approx 2Lh$ as interacting surface area and $\vec{v}$ as velocity of the movable electrodes.

$|\theta| > \theta_{\text{c}}$ The comb structure is fully disengaged. Since the distance between the electrodes is still small in comparison to the length and height, the resulting flow between them can be considered as HAGEN-POISEUILLE flow (Fig. 3b, [2]), indicated by a parabolic velocity profile. According to Eq. (12), the resulting damping force can be expressed by:

$$\vec{F}_{\text{d}} \approx \vec{F}_{\text{Poiseuille}} = -4 \, \eta_{\text{eff}} \, \frac{A_{\text{s}}}{d_{\text{h}}} \, \vec{v} \, \xi \tag{15}$$

with

$$\xi = \left(1 - \frac{|\vec{u}_0|}{|\vec{v}|} \right) \quad \text{and} \quad d_{\text{h}} = 4 \, \frac{A}{U}$$

$A \approx L(2g + b)$ is the hydraulic diameter, U is the perimeter of the flow channel.

$0 < |\theta| < \theta_{\text{c}}$ The comb structure is in transition between engaged and disengaged state. COUETTE flows as well as HAGEN-POISEUILLE flows are appearing between the electrodes.

3.2 Damping of mirror plate

In terms of damping mechanisms at tilting plates, two different effects have to be distinguished:

Drag damping is affecting every structure moving within a fluid. The damping forces result according to Eq. (12) from integration over pressure which can be described by NAVIER-STOKES equations (11):

$$\vec{F}_{\mathrm{drag}} \;=\; -\frac{\vec{v}}{|\vec{v}|}\; c_{\mathrm{d}}\, \rho_{\mathrm{m}}\; |\vec{v}|^2\; \frac{A_{\mathrm{p}}}{2} \qquad (16)$$

With A_{p} as base area of the mirror plate and c_{d} as empirical factor which can be determined by experiments or numerical analyses. From Eq. (13) we can derive the damping torque of a tilting plate caused by drag effects:

$$\vec{M}_{\mathrm{drag}} \;\approx\; -\frac{c_{\mathrm{d}}\, \rho_{\mathrm{m}}}{2}\; \vec{\omega}\; |\vec{\omega}| \iint\limits_{(A_{\mathrm{p}})} |\vec{r}|^3\; dA \qquad (17)$$

With $\vec{\omega} = \dot{\vec{\theta}}$ as angular velocity of the mirror plate (Fig. 4). It should be noted that the daming torque depends quadratically on the angular velocity $\vec{\omega}$. Since $|\vec{\omega}| \propto f\hat{\theta}$, a growing influence of drag damping can be expected for micromirrors with high frequencies or deflection angles.

Squeeze film damping occurs when a plate is moving nearby a immovable structure (e.g. according to Fig. 4). A changing distance results in a progression of pressure and leads to a flow between the plate and the structure. Since IPMS micromirrors usually have a small cavity underneath the mirror plate this effect can also be relevant for a damping analysis. For small distances between plate and immovable structure the squeeze film effect can be described by an analytical approximation [3, 5]:

$$\frac{\partial^2 p'}{\partial x^2} + \frac{\partial^2 p'}{\partial y^2} \;=\; 12\, \frac{\eta_{\mathrm{eff}}}{d^3}\, v_z\;, \quad p'_{\mathrm{bc}} = 0 \qquad (18)$$

In this POISSON's differential equation $v_z = f(x, y)$ is the velocity of the plate in direction of its normal, $p' = p - p_0$ is the difference between pressure and ambient pressure. Analogical to Eq. (13) the damping torque resulting from the squeeze film effect can by expressed by:

$$M_{\mathrm{sq}} \;=\; \iint\limits_{(A_{\mathrm{p}})} p'\, y\; dA \qquad (19)$$

Solutions of Eq. (18) for simple geometries and examples of resulting pressure regimes can be found in [3].

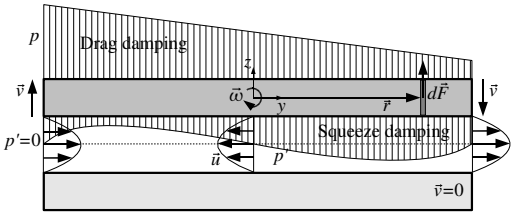

Figure 4: Damping mechanisms of tilting plates

4 Numerical model

To verify analytical approaches and for determination of flow parameters ξ in Eq. (15) as well as c_{d} in Eq. (17) numerical models are required. Two numerical models are created using the FEM tool *COMSOL Multiphysics*^{TM}, utilizing the application mode *Incompressible Navier-Stokes*.

4.1 Comb drive

In order to perform damping analyses of arbitrary IPMS microscanners, a parametrized finite element model of the out-of-plane comb is created. Comparisons of several two- and three-dimensional approaches using a complex reference model with three electrode fingers and their respective counter electrodes (left-hand side of Fig. 5) show that the model has to be three-dimensional to include all relevant effects. The final FEM model consists of a half finger and a half counter electrode (right-hand side of Fig. 5). Using symmetrical boundary conditions, the fluid state at an electrode which is contained in a electrode comb with infinite number of fingers, can be simulated. Since the count of electrodes is usually very high, the error caused by electrodes near the ends of the comb is assumed to be small.

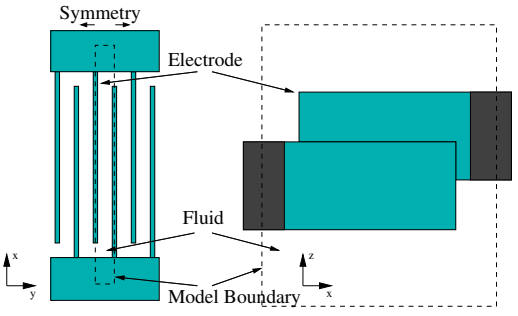

Figure 5: Fluidmechanical FEM model with symmetric boundary conditions

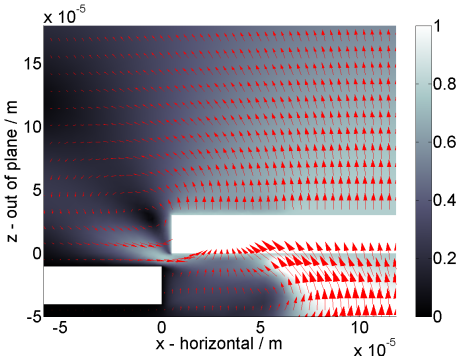

Figure 6: Velocity slice plot along the middle of a disengaged moving electrode

Figure 6 shows a typical slice plot of the velocity field of the fluid. Barring changes of the finger geometry and location, the FEM model has only two degrees of freedom: the finger velocity $\vec{v} = \vec{f}(\vec{\omega})$ and the deflection of the finger $s = f(\theta)$. Therefore the damping characteristic of a certain comb geometry at variable mirror dimensions, frequencies, and deflections can be completely investigated by exclusively considering variable velocity and deflection of the electrodes.

To prove the assumptions made in the analytic model, the velocity profiles between the electrodes are extracted. Thereby an interesting effect can be observed. The COUETTE flow as well as the HAGEN-POISEUILLE flow, both appear at the moving electrodes as expected, but additionally a second HAGEN-POISEUILLE flow develops between the counter electrodes (Fig. 7). This is caused by the moving electrode which acts like a piston, dragging the fluid. According to the law of actio and reactio the appearing shear forces at the counter electrode are applied by the moving electrode. This results in an additional damping force while the transition between engaged and disengaged state. Since two different Poiseuille flows have to be considered, two different factors ξ_1 and ξ_2 are required. Thereby, ξ_1 characterizes the flow between the counter electrodes and ξ_2 characterizes the flow between the moving electrodes. From simulations with variable deflections, the characteristics of ξ_1 and ξ_2 depending on s can be derived. Using this, it is possible to utilize Eq.(14) and Eq. (15) to realize a good approximation of the damping force of a moving electrode:

$$\vec{F}_\mathrm{d} \approx \vec{F}_\mathrm{Couette} + \sum \vec{F}_\mathrm{Poiseuille} \qquad (20)$$

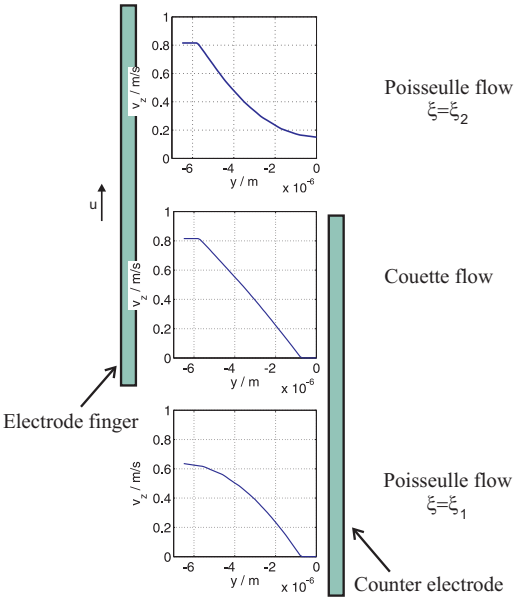

Figure 7: Simulated velocity profiles between moving electrodes and its counter electrodes

4.2 Mirror plate with cavity

Damping properties of the mirror plate can be investigated with a simplified 3D FEM model (Fig. 8). To reduce complexity the comb is not included. The tilting of the plate is considered by a location-dependent boundary condition: $u_{z,\mathrm{bc}} = v_{z,\mathrm{bc}} = y\,|\vec{\omega}|$.

The damping torque for a given angular velocity $\vec{\omega} = f(\theta, f)$ can be derived using the integration capabilities of *COMSOL Multiphysics*^{TM} according to Eq. (12) and Eq. (13) respectively.

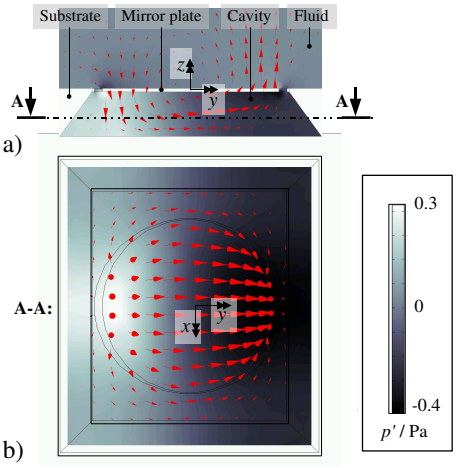

Figure 8: Simulation results for a 3D FEM model of a micromirror with standard cavity

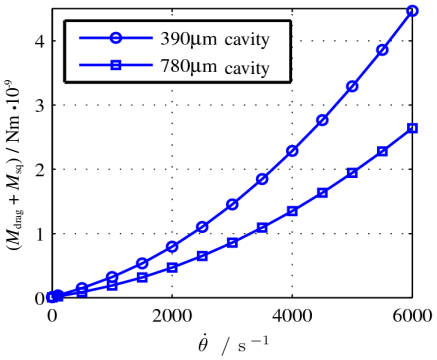

Figure 9: Damping torques for different cavities

Fig. 9 shows damping torques of a circular mirror plate with a diameter of 1.5 mm and two cavity heights. It is noticeable that the resulting curves are superpositions of linear and quadratic functions. By using nonlinear curve fitting, the empirical factor c_d can be derived as well as the linear damping coefficient caused by the squeeze film effect.

5 Experimental results

Utilizing Eq. (3), Eq. (13) and the values for the flow parameters ξ_1, ξ_2 and c_d according to section 4, it is possible to calculate the mean damping coefficient for a given deflection amplitude. Fig. 10 shows a comparison of simulated mean damping coefficients and experimental data. Although the simulated damping coefficients are consistently smaller, the characteristic is very similar. The difference can be explained by the unavoidably non-ideal driving regime used in the experimental setup [4]. Since the theoretical maximum amplitude can never be reached in the real world the damping coefficient is overestimated.

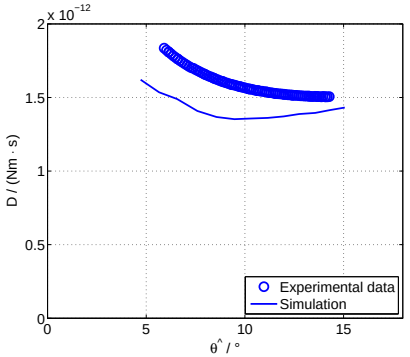

Figure 10: Mean damping coefficients

6 Conclusion

In this paper we presented a damping model for micromirrors with out-of-plane comb drive. The model bases on Navier-Stokes theory and includes the viscous gas damping within the comb drive as well as the effects caused by drag damping and squeeze film damping affecting the mirror plate. The validity limits of this model were discussed in terms of pressure and temperature changes and were proven by experimental data. The simulation results fit experimental results very well.

With the presented models and methods it is possible to predict the damping properties of arbitrary comb and mirror geometries. This is very important for understanding the behavior of available micromirrors. It is also a requirement for the optimization of this devices. Thereby the geometry of the comb drive, the geometry of the mirror plate and the cavity of the device can be varied in order to find an improved design.

References

[1] Mohamed Gad el Hak, *The mems handbook*, CRC Press, 2002.

[2] T. Klose, T. Sandner, H. Schenk, and H. Lakner, *Extended damping model for out-of-plane comb driven micromirrors*, SPIE Proceedings Series 6114 (2006), 184–195.

[3] J. Mehner, *Entwurf in der mikrosystemtechnik*, Dresden Univ. Press, 1999.

[4] T. Sandner, T. Klose, A. Wolter, H. Schenk, and H. Lakner, *Damping analysis and measurement for a comb-drive scanning mirror*, SPIE Proceedings Series 5455 (2004), 147–158.

[5] J. Starr, *Squeeze-film damping in solid-state accelerometers*, IEEE Solid-State Sensor and Actuator Workshop (1990).

[6] Timo Veijola, Heikki Kuisma, Juha Lahdenperä, and Tapany Ryhänen, *Equivalent-circuit model of the squeezed gas film in a silicon accelerometer*, Sensors and Actuators **A 48** (1995), 239–248.